

# Determining Energy Efficiency Sweet Spots in Production LLM Inference

Hiari Pizzini Cavagna\*  
 hiari.pizzinicavagna@unibo.it  
 University of Bologna  
 Bologna, Italy

Giovanni B. Esposito  
 g.esposito@unibo.it  
 University of Bologna  
 Bologna, Italy

Zeynep Kiziltan  
 zeynep.kiziltan@unibo.it  
 University of Bologna  
 Bologna, Italy

Andrea Proia\*  
 andrea.proia@unibo.it  
 University of Bologna  
 Bologna, Italy

Francesco Antici  
 francesco.antici@unibo.it  
 University of Bologna  
 Bologna, Italy

Giacomo Madella  
 giacomo.madella@unibo.it  
 University of Bologna  
 Bologna, Italy

Daniele Cesarini  
 d.cesarini@cineca.it  
 Cineca  
 Bologna, Italy

Andrea Bartolini  
 a.bartolini@unibo.it  
 University of Bologna  
 Bologna, Italy

## Abstract

Large Language Models (LLMs) inference is central in modern AI applications, making it critical to understand their energy footprint. Existing approaches typically estimate energy consumption through simple linear functions of input and output sequence lengths, yet our observations reveal clear Energy Efficiency regimes: peak efficiency occurs with short-to-moderate inputs and medium-length outputs, while efficiency drops sharply for long inputs or very short outputs, indicating a non-linear dependency. In this work, we propose an analytical model derived from the computational and memory-access complexity of the Transformer architecture, capable of accurately characterizing the efficiency curve as a function of input and output lengths. To assess its accuracy, we evaluate energy consumption using TensorRT-LLM on NVIDIA H100 GPUs across a diverse set of LLMs ranging from 1B to 9B parameters, including OPT, LLaMA, Gemma, Falcon, Qwen2, and Granite, tested over input and output lengths from 64 to 4096 tokens, achieving a mean MAPE of 1.79%. Our results show that aligning sequence lengths with these efficiency “Sweet Spots” can substantially reduce energy usage, supporting informed truncation, summarization, and adaptive generation strategies in production systems.

## Keywords

LLM Energy Consumption, Joules per Token, Inference costs

## 1 Introduction

Large Language Models (LLMs) have rapidly emerged as the foundation of modern Natural Language Processing (NLP), enabling applications ranging from reasoning and summarization to dialogue systems and generative AI. Their adoption at scale, however, has introduced a growing concern: the substantial energy consumption associated with inference, which is estimated to account for up to 90% of the model’s consumption [Jegham et al. 2025]. Unlike training, which is an episodic process, inference occurs continuously in production settings, every time an LLM generates output

for a user query. This shift makes inference efficiency a critical challenge for both sustainability and deployment cost.

A key contributor to inference complexity in LLMs is the attention mechanism. Since the original Transformer design [Vaswani et al. 2017], the standard Multi-Head Attention (MHA) has undergone several modifications aimed at improving efficiency. Variants such as Multi-Query Attention (MQA) [Shazeer 2019] and Grouped-Query Attention (GQA) [Ainslie et al. 2023] reduce memory requirements by sharing key-value projections across heads, thereby lowering the cost of maintaining and accessing the Key–Value (KV) cache during decoding. Recent studies [Dao et al. 2022] further highlight that attention kernels are often memory-bound rather than compute-bound, making their design a critical factor for inference efficiency at scale. These insights underscore the central role of attention in determining both the computational and energy footprint of LLM inference.

The energy consumption of LLM inference is shaped by a complex interplay of model size, architecture, and workload geometry (i.e., the distribution of input and output sequence lengths). While recent studies have examined inference energy consumption through empirical benchmarks [Fernandez et al. 2025], they often focus on specific models [Stojkovic et al. 2024] or high-level metrics such as latency and throughput [Maliakel et al. 2025]. Previous works [Wilkins et al. 2024] have assumed linear relation between the workload parameters ( $n_{in}$  = input tokens,  $n_{out}$  = output tokens) and the energy consumed by each generated token. Our characterization show a different result: the energy per token has local minima in  $n_{in}$  and  $n_{out}$  space, which can’t be explained by a linear model.

In this work, we propose an analytical model derived from the computational and memory access complexity of the Transformer, which captures the non-linear relationship between input and output sequence lengths. To evaluate our approach, we conduct a systematic analysis of LLM inference energy consumption using TensorRT-LLM, a state-of-the-art inference stack optimized for modern GPUs, running on NVIDIA H100 accelerators. Our study covers a broad set of models spanning from 1B to 9B parameters,

\*Both authors contributed equally to this research.

including OPT [Zhang et al. 2022], LLaMA [Grattafiori et al. 2024], Gemma [Team et al. 2024], Falcon [Almazrouei et al. 2023], Qwen2 [Yang et al. 2024], and Granite [Mishra et al. 2024], and explores efficiency across input and output lengths ranging from 64 to 4096 tokens.

Our contributions are threefold:

- We present an analytical model that explicitly relates energy consumption to the computational cost (measured in FLOPs) of inference. This formulation reveals how quadratic input costs and linear decoding costs combine to produce the efficiency patterns observed in practice. Furthermore, we also derive an additional formulation of the model, which integrates Memory access into the equation.
- We validate these models through extensive measurements across multiple LLM families, showing that the FLOPs and Memory Access based model accurately captures the location of efficiency Sweet Spots as a function of input and output lengths, achieving a mean MAPE of 1.79% ( $\pm 0.61$ ).
- We demonstrate that efficiency is not monotonically dependent on input or output sequence lengths. Instead, it exhibits distinct regimes: peak efficiency occurs for short-to-medium inputs combined with medium outputs, while efficiency sharply declines for long inputs or very short outputs, with Sweet Spot efficiency exceeding the worst-case setting by a factor of 33.41 $\times$ .

Our results suggest that production deployments can optimize Energy Efficiency by tailoring batching strategies, truncating overly long inputs, or aligning output lengths with the efficiency Sweet Spots predicted by our model.

The rest of the paper is organized as follows. After giving the necessary background in Section 2, we review related work in Section 3. Then in Sections 4 and 5 we present our analytical models and experimental methodology, before we present our experimental results in Section 6. We discuss our findings in Section 7 and conclude in Section 8.

## 2 Background

### 2.1 LLMs Architecture

LLMs are based on the Transformer architecture [Vaswani et al. 2017], which has become the standard for generative AI. A transformer block is composed of two main components: the Multi-Head self-Attention mechanism (MHA) and the Feed-Forward Network (FFN), both surrounded by residual connections, layer normalization, and dropout. The attention mechanism is commonly implemented as MHA, where the hidden representation is projected into different subspaces (heads). Each head learns to capture different types of dependencies in the sequence, and their outputs are later combined. While this improves the model’s expressivity and ability to represent diverse relationships, it also increases the total number of operations roughly in proportion to the number of heads. To reduce this overhead, Multi-Query Attention (MQA) was proposed in 2019 [Shazeer 2019], modifying MHA by keeping multiple query heads but sharing a single set of KV projections across all heads. This design drastically reduces memory usage and KV cache size during decoding, making inference more efficient. More recently, Grouped-Query Attention (GQA) was introduced in 2023 [Ainslie

et al. 2023] as a generalization of MHA and MQA: keys and values are shared within groups of heads, striking a balance between the efficiency of MQA and the expressivity of MHA.

### 2.2 LLMs Computation

In large-scale models, the majority of parameters reside in the FFN layers, while the attention mechanism dominates runtime complexity due to its quadratic dependence on the input sequence length. LLM inference is typically divided into two phases: *prefill*, where the full input sequence is processed in parallel to initialize the KV cache; and *decode*, where tokens are generated autoregressively. In the prefill stage, the computational cost is dominated by the quadratic attention term, whereas in the decode stage, the cost per token is linear with respect to the sequence length, due to the reuse of cached keys and values. Despite this, the decode phase often dominates total inference time for long outputs, as each token must be produced sequentially, limiting opportunities for parallelization. On modern GPUs, the throughput of LLM inference is not solely limited by arithmetic performance but also by memory bandwidth. Storing and retrieving the large KV cache during decoding creates significant pressure on the memory subsystem with high bandwidth requirements. For instance, in autoregressive decoding, each generated token requires the loading of all previous keys and values from memory, resulting in attention kernels being strongly memory-bound, particularly for long contexts [Yuan et al. 2024].

### 2.3 Inference Frameworks

When it comes to executing LLM inference on production hardware, several software runtimes exist, such as TensorRT-LLM [NVIDIA 2025], vLLM [Kwon et al. 2023] and DeepSpeed [Aminabadi et al. 2022], each offering different levels of optimization and targeting different deployment constraints. These runtimes vary substantially in how they manage memory, parallelize attention, and schedule kernels. TensorRT-LLM focuses on graph-level optimizations and low-level kernel fusion, vLLM is an open-source inference system explicitly tailored for high-throughput LLM serving. Its main contribution, the PagedAttention mechanism, improves memory efficiency by partitioning key-value caches, thereby enabling scalable batch inference with reduced memory overhead. DeepSpeed, developed by Microsoft, provides a distributed training and inference framework aimed at maximizing scalability using techniques such as the Zero Redundancy Optimizer [Rajbhandari et al. 2020].

**2.3.1 TensorRT-LLM.** In particular, TensorRT-LLM is NVIDIA’s specialized inference framework designed for optimizing LLM serving on modern GPUs. It builds upon the TensorRT optimization stack, extending it with kernels and execution strategies tailored for transformer-based architectures. The framework provides a toolchain that converts pretrained models into highly optimized TensorRT engines. This process includes parsing the original model graph, applying operator fusion, and lowering precision to FP16, BF16, or INT8 when supported. Once converted, the engine is serialized and can be executed through the TensorRT runtime, which is tightly integrated with CUDA and NVIDIA’s kernel libraries. Compared to general-purpose libraries, TensorRT-LLM provides a lower-level execution model where computational and memory

operations are highly optimized for modern GPUs (e.g., NVIDIA’s Hopper architecture).

Beyond these system-level design advantages, recent empirical evidence further motivates the use of TensorRT-LLM. In particular, the authors of [Niu et al. 2025] present a comparative analysis of the frameworks mentioned above, and finds that vLLM and TensorRT-LLM consistently achieves the most energy efficient token generation among the compared frameworks, especially under high-concurrency and high-throughput workloads. Component-level measurements additionally show that both vLLM and TensorRT-LLM consumes about the 5% GPU energy with respect to the consumption of a general-purpose serving frameworks as Transformers [Wolf et al. 2020], demonstrating how its hardware-aware optimizations translate directly into power savings. Collectively, these results show that TensorRT-LLM is not only engineered for performance but is also empirically validated as one of the most energy-efficient inference engines available. Based on the above consideration and to obtain production-grade figure of merit we choose TensorRT-LLM as inference run-time in this paper. Future works will extend the analysis on different ones.

**2.3.2 In-Flight Batching.** A key runtime optimization employed by TensorRT-LLM to maximize throughput under dynamic workloads is its *in-flight batching* strategy. Unlike static batching, where requests must be grouped prior to execution and processed synchronously, in-flight batching enables the runtime to continuously merge and schedule requests that are already undergoing inference. This mechanism is particularly well suited for autoregressive LLM decoding, where sequences progress token by token and naturally diverge in length. At a high level, TensorRT-LLM decouples request admission from kernel execution. Incoming inference requests are first tokenized and then admitted into an active set of sequences maintained by the runtime scheduler. During each decoding iteration, TensorRT-LLM dynamically forms micro-batches composed of all active sequences that are ready to generate the next token. Newly arriving requests can be inserted into this active set without waiting for the completion of previous batches, while completed sequences are removed as soon as they reach their termination condition. As a result, GPU execution remains continuously occupied, reducing idle cycles that would otherwise arise from batch fragmentation. From a systems perspective, in-flight batching trades strict per-request latency determinism for significantly improved throughput and hardware utilization, being especially effective in production serving scenarios, where request arrival times and sequence lengths are inherently unpredictable.

The behavior of in-flight batching is governed by user-configurable limits, notably `max_batch_size` and `max_num_tokens`. The `max_batch_size` parameter specifies the maximum number of active requests that can be scheduled concurrently in a decoding iteration, effectively bounding the degree of request-level parallelism. In contrast, `max_num_tokens` constrains the total number of tokens processed in a single micro-batch, aggregating across all active sequences. This token-level limit is particularly important for controlling GPU memory usage per iteration.

### 3 Related Work

Several recent works have characterized and modeled the energy footprint of LLM inference. [Fernandez et al. 2025] presents a systematic analysis of inference efficiency optimizations across diverse NLP and generative AI workloads, considering input–output token distributions, batching strategies, GPU hardware, software frameworks, and decoding methods. Their work shows that real-world energy consumption is highly sensitive to workload geometry and software–hardware configurations.

Authors of [Niu et al. 2025] characterize the power consumption of different inference engines (Transformers, vLLM, DeepSpeed, and TensorRT-LLM). They compute the Energy-per-Token metric  $E_{\text{tok}}$  as:

$$E_{\text{tok}} = \frac{E_{\text{tot}}}{n_{\text{out}}}, \quad (1)$$

where  $E_{\text{tot}}$  is the total energy consumption during inference and  $n_{\text{out}}$  the total generated output tokens.

In [Wilhelm et al. 2025] they investigate the trade-offs between accuracy and energy consumption when applying test-time compute strategies. They propose energy-aware routing mechanisms to guide sustainable model selection and inference, defining  $E_{\text{tok}}$  as:

$$E_{\text{tok}} = \frac{E_{\text{tot}}}{n_{\text{out}} + n_{\text{in}}}. \quad (2)$$

Finally, in [Wilkins et al. 2024] they characterize the energy consumption and runtime behavior of a set of LLMs using A100 GPUs, proposing workload-based energy models that, for a given model, predict consumption as a function of only the input and output tokens. To the best of our knowledge, this is the only work that proposes a model to describe the total energy consumption as a function of input and output token as follows:

$$E_{\text{tot}} = \theta_0 n_{\text{in}} + \theta_1 n_{\text{out}} + \theta_3 n_{\text{in}} n_{\text{out}}. \quad (3)$$

In contrast to these studies, we introduce an analytical model of LLM inference energy consumption derived from both computational and memory-access complexity, enabling us to characterize the nonlinear interplay between input and output sequence lengths. To assess this model, we perform a systematic study of inference energy usage using TensorRT-LLM on NVIDIA H100 GPUs, covering a diverse set of models and spanning a wide range of sequence lengths. Our formulation makes explicit how quadratic input-processing costs and linear decoding costs combine to shape the efficiency patterns seen in practice, and we provide an extended version of the model that incorporates memory-access effects. Through extensive evaluation across multiple model families, we show that the analytical model closely reflects real energy trends and correctly identifies where efficiency peaks occur as a function of input and output lengths. Finally, we demonstrate that efficiency does not increase or decrease uniformly with sequence length but instead follows distinct regimes, with clear sweet spots and clear degradation zones depending on the balance between input size and output length.

**Table 1: Analytical Model Set**

Model	Formula
Baseline 1 [Niu et al. 2025]	$E_{\text{tok}} = \theta_0$
Baseline 2 [Niu et al. 2025]	$E_{\text{tok}}(n_{\text{out}}) = \theta_0 + \frac{\theta_1}{n_{\text{out}}}$
Baseline 3 [Wilhelm et al. 2025]	$E_{\text{tok}}(n_{\text{in}}, n_{\text{out}}) = \theta_0 + \frac{\theta_1}{n_{\text{in}} + n_{\text{out}}}$
Baseline 4 [Wilkins et al. 2024]	$E_{\text{tok}}(n_{\text{in}}, n_{\text{out}}) = \theta_0 + \frac{\theta_1 n_{\text{in}}}{n_{\text{out}}} + \theta_2 n_{\text{in}}$
FLOPs-based (Ours)	$E_{\text{tok}}(n_{\text{in}}, n_{\text{out}}) = \theta_0 + \frac{\theta_1 n_{\text{in}}^2}{n_{\text{out}}} + \theta_2 n_{\text{in}} + \frac{\theta_3 n_{\text{in}}}{n_{\text{out}}} + \theta_4 n_{\text{out}}$
Memory and FLOPs-based (Ours)	$E_{\text{tok}}(n_{\text{in}}, n_{\text{out}}) = \theta_0 + \frac{\theta_1 n_{\text{in}}^2}{n_{\text{out}}} + \theta_2 n_{\text{in}} + \frac{\theta_3 n_{\text{in}}}{n_{\text{out}}} + \theta_4 n_{\text{out}} + \frac{\theta_5}{n_{\text{out}}}$

## 4 LLM Inference Consumption Analytical Models

In this section, we present our analytical frameworks for modeling LLM energy consumption, explicitly analyzing the distinct computational characteristics of the *prefill* and *decode* phases. To assess the validity of our approach, we compare our proposed models against four baselines, summarized in Table 1. From [Niu et al. 2025] we derive Baseline 1, which simply describes the  $E_{\text{tok}}$  as constant. Moreover, we formalize a parametrized model that relies solely on the number of generated tokens,  $n_{\text{out}}$ , to characterize  $E_{\text{tok}}$ , referred to as Baseline 2. The third baseline, Baseline 3, expands on this by also including the number of input tokens,  $n_{\text{in}}$ , as introduced in Equation 2. This formulation allows us to establish a relationship between  $E_{\text{tok}}$  and the total sequence length. Finally, Baseline 4 is derived directly from Equation 3.

### 4.1 FLOPs-Based Model

To evaluate the Energy Efficiency of our LLMs, we derived an analytical model of the computational complexity of inference. The model accounts for both the *prefill* phase, where the entire input sequence is processed in parallel, and the *decode* phase, where tokens are generated autoregressively using the cached key-value (KV) states. In this section, we present the derivation of the formulas for each phase and then combine them into a unified expression. During the prefill stage, the model processes an input sequence of length  $n_{\text{in}}$  in parallel. For a single Transformer layer with hidden size  $d$ , the computational cost can be decomposed into two main contributions: the Self-Attention Mechanism and the Feed-Forward Network. We neglect the cost of scaling, softmax, layer normalization, dropout, and bias additions, which are negligible w.r.t. the cost of attention and FFN. Moreover, we adopt the standard FLOPs accounting convention where one multiply–accumulate operation is counted as two FLOPs (one multiplication and one addition).

#### 4.1.1 Prefill Stage FLOPs.

**Attention.** The attention mechanism involves the following matrix multiplications:

Input projections to  $Q, K, V$ : the input  $X \in \mathbb{R}^{n_{\text{in}} \times d}$  is multiplied by three weight matrices  $W_Q, W_K, W_V \in \mathbb{R}^{d \times d}$ :

$$F_{\text{proj}} = 3 \cdot (2n_{\text{in}}d^2) = 6n_{\text{in}}d^2.$$

This corresponds to three dense matrix multiplications of size  $n_{\text{in}} \times d$  by  $d \times d$ .

Attention score computation  $QK^T$ : multiplication of  $Q \in \mathbb{R}^{n_{\text{in}} \times d}$  with  $K^T \in \mathbb{R}^{d \times n_{\text{in}}}$ :

$$F_{QK^T} = 2n_{\text{in}}^2d.$$

Weighted sum with  $V$ : multiplication of the  $n_{\text{in}} \times n_{\text{in}}$  attention matrix with  $V \in \mathbb{R}^{n_{\text{in}} \times d}$ :

$$F_V = 2n_{\text{in}}^2d.$$

Final output projection: multiplication with  $W_O \in \mathbb{R}^{d \times d}$ :

$$F_{\text{out}} = 2n_{\text{in}}d^2.$$

Summing these terms yields the attention cost per layer:

$$F_{\text{att}}(n_{\text{in}}) = 8n_{\text{in}}d^2 + 4n_{\text{in}}^2d.$$

**FFN.** The feed-forward network expands the hidden dimension by a factor of 4, with two dense matrix multiplications per token:

$$F_{\text{FFN}}(n_{\text{in}}) = 8n_{\text{in}}d^2 + 8n_{\text{in}}d^2 = 16n_{\text{in}}d^2.$$

corresponding to  $XW_1$  and the subsequent  $W_2$  projection back to dimension  $d$ .

**Total Prefill.** For one layer:

$$F_{\text{prefil, layer}}(n_{\text{in}}) = 24n_{\text{in}}d^2 + 4n_{\text{in}}^2d.$$

For an  $L$ -layer model:

$$F_{\text{prefil}} = L \cdot (24n_{\text{in}}d^2 + 4n_{\text{in}}^2d).$$

**4.1.2 Decode Stage FLOPs.** At decoding step  $t$ , the model has access to  $n_{\text{in}} + t - 1$  cached tokens. For each new token, the per-layer costs are:

**Attention.** Projections for  $Q, K, V$ , and output: multiplications with  $d \times d$  weight matrices:

$$F_{\text{proj+out}} = 8d^2.$$

Attention with cached keys and values: multiplication of  $Q \in \mathbb{R}^{1 \times d}$  with cached  $K^T \in \mathbb{R}^{d \times (n_{\text{in}}+t-1)}$  and multiplication of resulting attention scores with  $V \in \mathbb{R}^{(n_{\text{in}}+t-1) \times d}$ :

$$F_{QK+V} = 4(n_{\text{in}} + t - 1)d.$$

**FFN.** Per token, the FFN again involves two  $d \times d$  multiplications:

$$F_{\text{FFN}} = 16d^2.$$

**Total per Token.** The per-token cost for one layer is therefore:

$$F_{\text{decode, layer}}(t) = 24d^2 + 4(n_{\text{in}} + t - 1)d.$$

**Total Decode.** Summing over  $n_{\text{out}}$  generated tokens and multiplying by  $L$  layers:

$$F_{\text{decode}} = L \sum_{t=1}^{n_{\text{out}}} (24d^2 + 4(n_{\text{in}} + t - 1)d) \\ = L(24n_{\text{out}}d^2 + 4d(n_{\text{out}}n_{\text{in}} + \frac{n_{\text{out}}(n_{\text{out}}-1)}{2})).$$

**4.1.3 Total Inference FLOPs.** By summing the Prefill and Decode FLOPs, we obtain:

$$F_{\text{total}}(n_{\text{in}}, n_{\text{out}}) = F_{\text{prefill}} + F_{\text{decode}} \\ = L \left[ 24d^2(n_{\text{in}} + n_{\text{out}}) + 4d(n_{\text{in}}^2 + n_{\text{out}}n_{\text{in}} + \frac{n_{\text{out}}(n_{\text{out}}-1)}{2}) \right].$$

We factor out the common multiplier  $2Ld$  and manipulate the formula to spot individual contributors. This compact form is convenient for later normalization to build the final model.

$$F_{\text{total}}(n_{\text{in}}, n_{\text{out}}) = 2Ld \left( 12d n_{\text{in}} + 12d n_{\text{out}} + 2n_{\text{in}}^2 + 2n_{\text{out}}n_{\text{in}} + n_{\text{out}}^2 - n_{\text{out}} \right).$$

We note that the external factors  $L$  and  $d$  depends only on model size (depth and width) and are constant for a given model. Since our goal is to capture how efficiency varies as a function of the input length  $n_{\text{in}}$  and the output length  $n_{\text{out}}$ , we remove this constant multipliers and express the energy as a linear combination of polynomial terms in  $n_{\text{in}}$  and  $n_{\text{out}}$ .

$$E_{\text{tot}}(n_{\text{in}}, n_{\text{out}}) = \theta_0 n_{\text{out}} + \theta_1 n_{\text{in}}^2 + \theta_2 n_{\text{out}}n_{\text{in}} + \theta_3 n_{\text{in}} + \theta_4 n_{\text{out}}^2 + \theta_5 n_{\text{out}}.$$

This formulation highlights the individual contributions of input length, output length, and their interaction. The learned parameters  $\theta_i$  capture the proportionality between the theoretical FLOP terms and the actual measured energy in Joules.

To analyze the computational cost on a *per-output-token* basis, we divide the total energy by the number of generated tokens  $n_{\text{out}}$ . This provides the average energy required to produce a single token, which is useful for comparing efficiency across different input–output configurations. By aggregating  $\theta_5$  to  $\theta_0$ , we obtain:

$$E_{\text{tok}}(n_{\text{in}}, n_{\text{out}}) = \theta_0 + \frac{\theta_1 n_{\text{in}}^2}{n_{\text{out}}} + \theta_2 n_{\text{in}} + \frac{\theta_3 n_{\text{in}}}{n_{\text{out}}} + \theta_4 n_{\text{out}}. \quad (4)$$

This normalized form highlights how the cost of processing the input sequence  $n_{\text{in}}$  is amortized across the output tokens, while the terms proportional to  $n_{\text{out}}$  reflect the per-token cost of decoding.

## 4.2 Memory and FLOPs-based Model

While FLOPs capture the arithmetic workload of inference, modern accelerators increasingly operate in a regime where energy consumption is dominated not by computation but by memory traffic, in particular the movement of activations, weights, and KV-cache tensors across the memory hierarchy. To accurately model energy, we therefore incorporate the memory-access cost alongside the computational cost derived in the previous section. In the following subsections, we present an analytical decomposition of the memory contribution during both the prefill and decode phases. As before, we analyze a single Transformer layer with hidden dimension  $d$  and input length  $n_{\text{in}}$ , and  $n_q$  number of heads. We again omit the negligible contributions of bias reads, layer-normalization reads/writes, and softmax.

**4.2.1 Prefill Stage Memory Operations.** During prefill, the model processes the entire sequence in parallel, producing input projections and attention tensors. Memory traffic arises from reading inputs, writing intermediate projected representations and attention matrices. For one layer, the total memory movement is decomposed as follows.

**Attention.** The attention mechanism involves the following memory transfers:

Input projections to  $Q, K, V$ : reading  $X \in \mathbb{R}^{n_{\text{in}} \times d}$  and writing projected tensors:

$$M_{\text{proj}} = 2n_{\text{in}}d + d^2.$$

Attention score computation  $QK^T$ : reading  $Q \in \mathbb{R}^{n_{\text{in}} \times d}$  and  $K^T \in \mathbb{R}^{d \times n_{\text{in}}}$  and writing the  $n_{\text{in}} \times n_{\text{in}}$  attention matrix:

$$M_{QK^T} = 2n_{\text{in}}d + n_{\text{in}}^2 n.$$

Weighted sum with  $V$ : reading the attention matrix and  $V \in \mathbb{R}^{n_{\text{in}} \times d}$  ( $n_q$  = number of heads):

$$M_V = 2n_{\text{in}}d + n_{\text{in}}^2 n_q.$$

Final output projection: reading the attention output ( $n_{\text{in}} \times d$ ) and writing the output representation:

$$M_{\text{out}} = 2n_{\text{in}}d + d^2.$$

Summing these terms gives the total attention memory per layer during prefill:

$$M_{\text{att}}(n_{\text{in}}) = 8n_{\text{in}}d + 2d^2 + 2n_{\text{in}}^2 n_q.$$

**FFN.** The feed-forward network reads the input activations, accesses its two weight matrices, and writes the intermediate expanded representation:

$$M_{\text{FFN}}(n_{\text{in}}) = 2n_{\text{in}}d + 8d^2.$$

**Total Prefill.** For an  $L$ -layer model:

$$M_{\text{prefill}} = L(M_{\text{att}} + M_{\text{FFN}}) = L(10n_{\text{in}}d + 10d^2 + 2n_{\text{in}}^2 n_q).$$

**4.2.2 Decode Stage Memory Operations.** Similarly to the FLOPs Decoding stage, at each step  $t$ , we describe the per-layer memory operations as follows.

**Attention.** Projections for  $Q, K, V$ , and output: multiplications with  $d \times d$  weight matrices:

$$M_{\text{proj+out}} = 2(2d + d^2).$$

Attention with cached keys and values: multiplication of  $Q \in \mathbb{R}^{1 \times d}$  with cached  $K^T \in \mathbb{R}^{d \times (n_{\text{in}}+t-1)}$  and multiplication of resulting attention scores with  $V \in \mathbb{R}^{(n_{\text{in}}+t-1) \times d}$ :

$$M_{QK^T+V} = 2((n_q + d)(n_{\text{in}} + t - 1) + d).$$

**FFN.** Per token, the FFN again involves two  $d \times d$  multiplications:

$$M_{\text{FFN}} = 2d + 8d^2.$$

**Total per Token.** The per-token cost for one layer is therefore:

$$M_{\text{decode, layer}}(t) = M_{\text{proj+out}} + M_{QK^T+V} + M_{\text{FFN}} \\ = 7d + 10d^2 + (n_q + d)(n_{\text{in}} + t - 1).$$

**Total Decode.** Summing over  $n_{\text{out}}$  generated tokens and multiplying by  $L$  layers:

$$M_{\text{decode}} = L \sum_{t=1}^{n_{\text{out}}} (7d + 10d^2 + (n_q + d)(n_{\text{in}} + t - 1)) \\ = L(7dn_{\text{out}} + 10d^2 n_{\text{out}} + (n_q + d)(n_{\text{in}} n_{\text{out}} + \frac{n_{\text{out}}(n_{\text{out}}-1)}{2})).$$

**4.2.3 Total Memory Operations.** By summing the Prefill and Decode Memory Operations, we obtain:

$$\begin{aligned} M_{\text{total}}(n_{\text{in}}, n_{\text{out}}) &= M_{\text{prefill}} + M_{\text{decode}} \\ &= L \left[ 10n_{\text{in}}d + 10d^2 + 2n_{\text{in}}^2 n_q \right. \\ &\quad \left. + n_{\text{out}} (7d + 10d^2 + (n_q + d)(n_{\text{in}} + \frac{(n_{\text{out}}-1)}{2})) \right]. \end{aligned}$$

As for the FLOPs-based model, we express the energy consumption as a linear combination of polynomial terms in  $n_{\text{in}}$  and  $n_{\text{out}}$ :

$$E_{\text{tot}}(n_{\text{in}}, n_{\text{out}}) = \theta_0 n_{\text{out}} + \theta_1 n_{\text{in}}^2 + \theta_2 n_{\text{out}} n_{\text{in}} + \theta_3 n_{\text{in}} + \theta_4 n_{\text{out}}^2 + \theta_5 n_{\text{out}} + \theta_6.$$

Relative to the  $E_{\text{tot}}$  of the FLOPs model, this formulation introduces an additional constant term,  $\theta_6$ . This term accounts for the contribution arising from the  $10d^2$  component in the  $M_{\text{prefill}}$  expression, which is independent of both  $n_{\text{in}}$  and  $n_{\text{out}}$ . Analyzing the energy consumption *per-output-token* and aggregating  $\theta_5$  to  $\theta_0$ , we obtain:

$$E_{\text{tok}}(n_{\text{in}}, n_{\text{out}}) = \theta_0 + \frac{\theta_1 n_{\text{in}}^2}{n_{\text{out}}} + \theta_2 n_{\text{in}} + \frac{\theta_3 n_{\text{in}}}{n_{\text{out}}} + \theta_4 n_{\text{out}} + \frac{\theta_5}{n_{\text{out}}}. \quad (5)$$

### 4.3 Energy Efficiency Sweet Spots

Using the computational model introduced in Equation 5, we identify energy-efficiency Sweet Spots by considering the per-token energy as a function of the number of generated tokens  $n_{\text{out}}$ . To this end, we compute the derivative of  $E_{\text{tok}}$  with respect to  $n_{\text{out}}$  and set it equal to zero:

$$\frac{\partial E_{\text{tok}}}{\partial n_{\text{out}}} = -\frac{\theta_1 n_{\text{in}}^2 + \theta_3 n_{\text{in}} + \theta_5}{n_{\text{out}}^2} + \theta_4. = 0$$

Solving for  $n_{\text{out}}$ , we obtain:

$$\begin{aligned} \frac{\theta_1 n_{\text{in}}^2 + \theta_3 n_{\text{in}} + \theta_5}{n_{\text{out}}^2} = \theta_4 \quad \Rightarrow \quad n_{\text{out}}^2 = \frac{\theta_1 n_{\text{in}}^2 + \theta_3 n_{\text{in}} + \theta_5}{\theta_4} \quad \Rightarrow \\ n_{\text{out}}^* = \sqrt{\frac{\theta_1 n_{\text{in}}^2 + \theta_3 n_{\text{in}} + \theta_5}{\theta_4}} \end{aligned} \quad (6)$$

This result shows that the per-token energy is minimized when the number of generated tokens is equal to the square root of a combination of the input sequence length and its quadratic contribution, normalized by the linear per-token decoding cost  $\theta_4$ .

## 5 Experimental Methodology

This section details the experimental methodology adopted to validate the proposed analytical models and to characterize the energy consumption of LLMs on modern hardware. We first describe the monitoring framework employed for the data acquisition. Next, we outline the selection of LLMs, ensuring a diverse representation of sizes and attention mechanisms. Next, we define the quantitative metrics used to assess Energy Efficiency and validate our theoretical derivations. Finally, we present the configurations for the dataset generation, engine building process and benchmark execution.

### 5.1 Monitoring Framework

The monitoring framework is designed to collect and analyze GPU metrics during LLM execution. In particular, hardware metrics such as `nvmlDeviceGetPowerUsage` and `NVML_CLOCK_GRAPHICS` are sampled using the NVIDIA Management Library Python API (`pynvml` [Corporation 2025]). These metrics are sampled at 500 ms

**Table 2: LLM test set grouped into size-based families (1B–9B), with architectural details for each model.**

Name	Size (B)	Heads-Attention	Hidd. Size	Layers
<b>XS models (From 1B to 1.5B)</b>				
Llama 3.2	1	32 - GQA (4x)	2048	16
OPT	1.3	32 - MHA	2048	24
Qwen 2	1.5	12 - GQA (6x)	1536	28
<b>S models (From 2B to 3B)</b>				
Gemma 2	2	8 - GQA (2x)	2304	26
OPT	2.7	32 - MHA	2560	32
Llama 3.2	3	24 - GQA (4x)	3072	28
Granite	3	32 - MHA	2048	32
<b>M models (From 6.7B to 9B)</b>				
OPT	6.7	32 - MHA	4096	32
Qwen 2	7	28 - GQA (7x)	3584	28
Falcon-RW	7.5	64 - MHA	4096	36
Granite	8	32 - GQA (4x)	4096	36
Llama 3.1	8	32 - GQA (4x)	4096	32
Gemma 2	9	16 - GQA (2x)	3584	42

intervals, published through the ExaMon plugin, and stored in the ExaMon database. For both data collection and transmission we employ an updated version of ExaMon [Bartolini et al. 2019], based on IoTDB Database [Wang et al. 2025].

### 5.2 LLM Selection

We consider a diverse set of LLMs, spanning from 1B to 9B parameters, as summarized in Table 2. In addition to model size, the selection includes architectures with different design choices and attention mechanisms—such as Multi-Head, Grouped-Query, and Multi-Query Attentions. To facilitate comparison, the models are grouped into three size-based families, ranging from XS models (1B–1.5B) to M models (6.7B–9B).

### 5.3 Metrics and Measurement

We quantify the energy consumption  $E_{\text{tot}}$  as the discrete integration of the mean instantaneous GPU power, measured as described in subsection 5.1 over the measurement interval  $\Delta t$ , according to the following expression:

$$E_{\text{tot}} = \sum_i \left( \frac{P_i + P_{i+1}}{2} \right) \Delta t,$$

where  $P_i$  denotes the power usage recorded at each time step  $i$ . We empirically obtain the Energy-per-Token  $E_{\text{tok}}$  by normalizing the energy consumption for the total amount of output tokens  $n_{\text{out}}$ :

$$E_{\text{tok}} = \frac{E_{\text{tot}}}{n_{\text{out}}} \quad \left[ \frac{\text{Joules}}{\text{Token}} \right].$$

For improved interpretability, we additionally define the LLM Energy Efficiency as the number of output tokens generated per unit of energy. Formally, this metric corresponds to the reciprocal of  $E_{\text{tok}}$ :

$$E_{\text{eff}} = \frac{n_{\text{out}}}{E_{\text{tot}}} \quad \left[ \frac{\text{Tokens}}{\text{Joule}} \right].$$

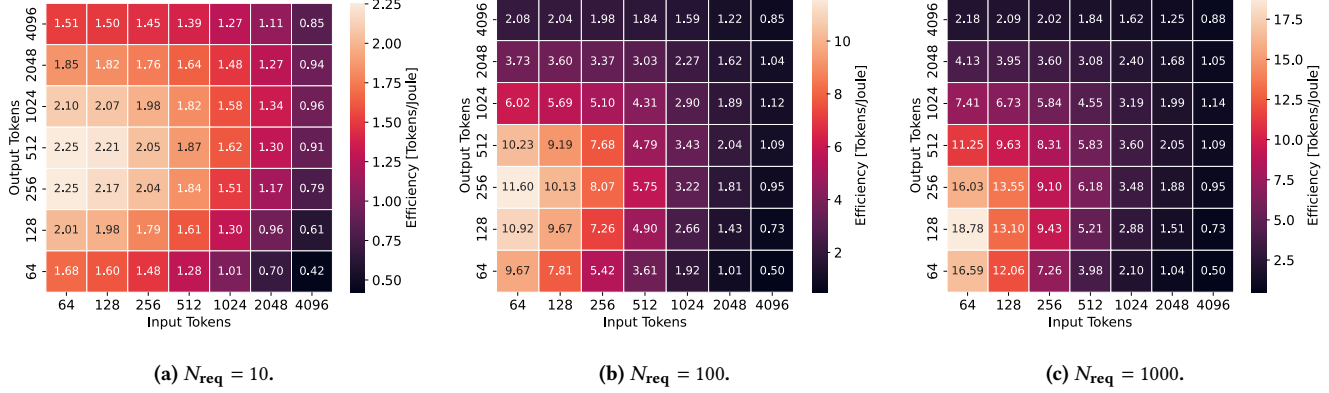


**Figure 1: Energy Efficiency  $\frac{\text{Tokens}}{\text{Joule}}$  of Falcon 7B with different number of requests (10,100,1000).**

This measure captures the productivity of the model with respect to its energy budget, facilitating clearer cross-model comparisons.

#### 5.4 Dataset Generation

To benchmark TensorRT-LLM under controlled and reproducible conditions, we generated synthetic request datasets using the official utility script provided with TensorRT-LLM. For each dataset, token sequences were sampled using the Llama-3.1-8B-Instruct tokenizer, with input and output lengths drawn from fixed distributions defined by a specified mean and zero variance. This allowed us to precisely control the number of input and output tokens per request. We generated datasets for all combinations of input and output lengths ranging from 64 to 4096 tokens (in powers of two), and for different workload sizes with the number of requests set to 10, 100, and 1000.

#### 5.5 Engines Configuration

All TensorRT-LLM engines used in our benchmarks were built using the `trtllm-bench` build, which converts model checkpoints into TensorRT-LLM engines. Engines were constructed with tensor parallelism and pipeline parallelism both set to one, ensuring single-GPU execution and isolating inference performance from inter-device communication effects. The maximum supported sequence length was set to 8192 tokens, allowing all benchmarked input–output combinations to execute within a single engine configuration without triggering engine rebuilds. Additionally, we configured the `max_batch_size` to 1024 and the `max_num_tokens` to 8192. This approach ensures that performance differences observed across experiments are attributable to workload characteristics rather than changes in engine structure or parallelization strategy.

#### 5.6 Benchmark Execution

Benchmark runs were executed with `trtllm-bench` in *throughput* mode, a dedicated TensorRT-LLM utility for evaluating LLM performance on a given dataset, designed to maximize sustained token generation rate under a fixed workload. Each run pairs a pre-built engine with a corresponding synthetic dataset, ensuring that model configuration and workload characteristics remain constant throughout the measurement. We first assessed different number

of requests (10, 100, and 1000). Subsequently, fixing the number of requests to 1000, we evaluated the LLMs listed in Table 2 while varying the input and output sequence lengths from 64 to 4096 tokens. By reusing the same engine across datasets and varying only the dataset parameters, the reported results isolate the impact of input/output length and request count on inference throughput.

## 6 Experimental Results

### 6.1 Setup

All experiments were conducted on a single-node server equipped with an *Intel® Xeon® Platinum 8480+* processor, belonging to the Sapphire Rapids family. In addition, the system hosts four NVIDIA H100 Tensor Core GPUs, connected through NVLink. The server is equipped with 32x64 GB of DDR5 RAM operating at a frequency of 4800 MHz. The system runs on a *Dell 00G41X Version A02* motherboard. The operating system is Alma Linux 9.5 with Linux kernel 5.14. The cooling infrastructure relies on a rack-mounted air cooling system with redundant fans, which operated at stable speeds of 5160 RPM during the experiments.

### 6.2 Number of Requests Selection

To assess the impact of the requests count  $N_{\text{req}}$  (i.e. the number of queries used for evaluation) on Energy Efficiency, we considered multiple workload sizes. We excluded the single-request setting because our monitoring framework introduces a non-negligible timing error, preventing reliable measurements in that regime where execution times are shorter.

Figure 1 shows the Energy Efficiency  $\frac{\text{Tokens}}{\text{Joule}}$  for the Falcon-RW 7B model. Different sub-figures refer to different evaluation workloads (10,100 and 1000). Each plot reports the average Energy Efficiency for different LLM inference, each with a different  $n_{\text{out}}$  (x-axis) and  $n_{\text{in}}$  (y-axis) configurations. As shown in the figure, the workload size strongly affects both the absolute efficiency values and their overall trends. In particular, the efficiency peak shifts toward larger output lengths when using fewer requests, a behavior driven by the reduced number of tokens processed per inference step. Furthermore, the spread between the highest and the lowest efficiency values narrows for smaller workloads. Specifically, with 10 requests,

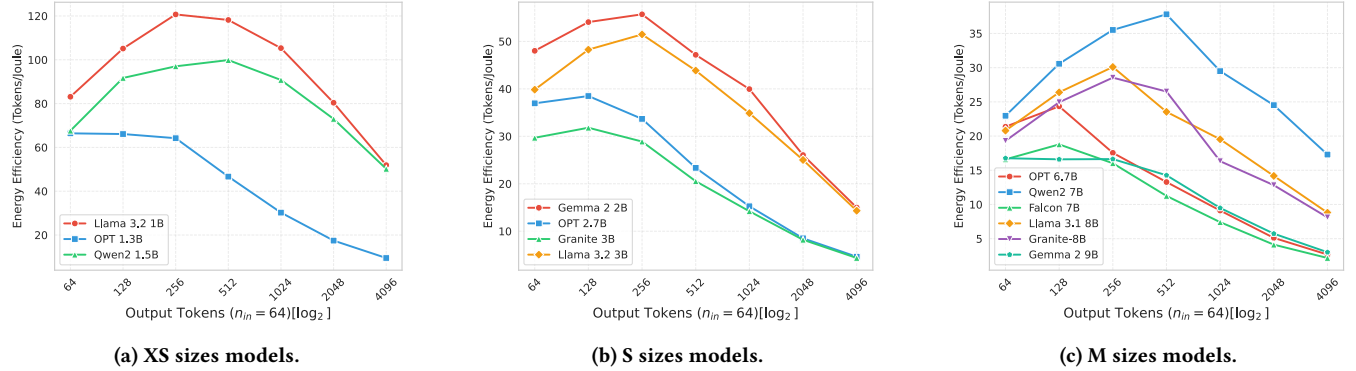


Figure 2: Energy Efficiency of tested LLM considering  $n_{in} = 64$  and varying output tokens, per size family (XS, S, M).

$E_{eff}$  ranges from 0.42 to 2.25, which consists in an increase of about 6 $\times$ . In contrast, with 1000 requests, the values range from 0.50 to 18.78, corresponding to a significantly wider gap of approximately 37.6 $\times$ .

Finally, smaller workloads amplify the relative impact of measurement overhead and necessitate shorter sampling intervals, which can further amplify measurement noise and result in less reliable estimates. For these reasons, in the subsequent experiments we focus on the saturation scenario and fix  $N_{req}$  at 1000. A more detailed analysis of how workload size interacts with batch-size is deferred to subsection 8.2.

### 6.3 Energy Efficiency Evaluation

In Figure 2 we show the Energy Efficiency [ $\frac{\text{Tokens}}{\text{Joule}}$ ] for each LLM for our test set, reported in Table 2, considering a fixed input length of  $n_{in} = 64$ . The sub-figures correspond to different LLM size families (XS, S, M), and illustrate how Energy Efficiency (y-axis) varies with the output length  $n_{out}$  (x-axis). As shown, different LLMs exhibit a substantial spread in  $E_{eff}$ . For instance, LLama 3.2 1B results the most efficient LLM, reaching 120.71 at  $n_{out} = 256$  and 51.90 at  $n_{out} = 4096$ , whereas Falcon RW 7B results the least efficient, with a Energy Efficiency values of 18.78 and 2.18 at the same output lengths. While the absolute efficiency values differ across models due to architectural differences, the overall behavior is consistent: each model exhibits a non-linear curve with a distinct peak in efficiency.

To highlight this common trend, we construct an aggregated heatmap (Figure 3) by applying min–max normalization to the efficiency values of each LLM and then averaging across the full set. The resulting 3D visualization reports the Energy Efficiency (z-axis), bounded between 0 and 1, and illustrates how it varies with different output lengths (x-axis) and input lengths (y-axis). This representation reveals a consistent non-linear pattern: the highest efficiency occurs at  $n_{in} = 64$  and  $n_{out} \in [128, 256]$ , whereas the lowest efficient is observed for shortest output lengths  $n_{out} = 64$  combined with the longest input length  $n_{in} = 4096$ . These results suggest the existence of “Sweet Spots” where LLMs achieve the best trade-off between energy consumption and token generated. Quantitatively, comparing for each model the worst efficient tokens combination, always located at the larger input and shorter output,

Table 3: Mean Absolute Percentage Error (MAPE) achieved by each analytical and baseline model across the LLMs of the test set.

Model	Baseline 1	Baseline 2	Baseline 3	Baseline 4	FLOPs based	Memory and FLOPs based
<b>XS models</b>						
Llama 3.2 (1B)	102.33	99.45	93.58	17.84	2.95	1.56
OPT (1.3B)	139.77	140.98	103.60	42.44	1.29	0.97
Qwen 2 (1.5B)	110.71	100.90	103.60	14.28	2.62	1.94
<b>S models</b>						
Gemma 2 (2B)	111.33	116.29	93.01	25.76	2.17	1.66
OPT (2.7B)	153.29	153.59	111.64	47.14	1.47	0.91
Llama 3.2 (3B)	117.54	121.55	99.77	24.19	2.46	2.12
Granite (3B)	144.28	148.05	107.43	42.44	1.85	1.08
<b>M models</b>						
OPT (6.7B)	151.27	155.47	110.08	46.49	1.82	1.93
Qwen 2 (7B)	132.26	113.34	126.04	15.26	3.24	2.88
Falcon-RW (7.5B)	150.80	155.75	109.90	47.30	1.48	1.35
Granite (8B)	127.92	128.22	111.45	24.32	2.62	2.24
Llama 3.1 (8B)	123.00	123.41	107.60	23.59	3.01	2.84
Gemma 2 (9B)	131.38	139.41	103.54	37.17	2.49	1.81
<b>Average</b>	<b>130.45</b>	<b>130.49</b>	<b>106.25</b>	<b>31.40</b>	<b>2.27</b>	<b>1.79</b>
<b>Std Dev</b>	<b>16.23</b>	<b>19.14</b>	<b>8.22</b>	<b>12.21</b>	<b>0.61</b>	<b>0.61</b>

with the highest efficiency Sweet Spot case (reported in Table 5), we observe on average a 33.41 $\times$  ( $\pm 4.90$ ) increase in efficiency across models. In Table 5 we also report every  $\theta$  for our Memory and FLOPs based model, and the estimated Sweet Spots, using the Equation 6.

### 7 Analysis and estimation of Energy Efficiency Sweet Spots

To estimate the Energy-per-Token  $E_{tok}$  for each combination of  $n_{in}$  and  $n_{out}$ , we fitted the state-of-the-art Baseline 1-4 and our proposed analytical models described in Table 1 with the results of the experiments of each LLM separately, using a non-linear least square method. In Table 3 we report the MAPE (Mean Absolute Percentage Error) for each analytical model fitted on the relative LLM.

From Table 3 we can notice that the proposed models FLOPs-based

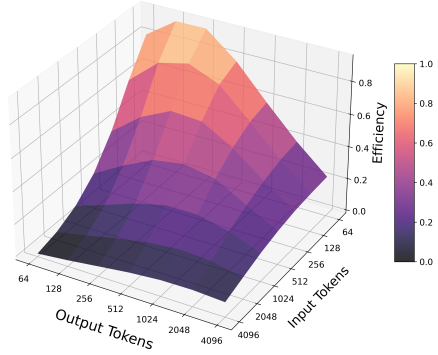


**Figure 3: Aggregated Energy Efficiency Heatmap.**

and Memory-and-FLOPs-based consistently achieves higher accuracy than the baselines for all the tested LLM inference models. In average, the Baseline 1 and 2 [Niu et al. 2025] achieves a MAPE of 130.45% and 130.49%, respectively. Baseline 3 [Wilhelm et al. 2025] improves the MAPE in average to the 106.25%, and Baseline 4 [Wilkins et al. 2024] further reduce it to 31.40%. This suggests that adding both  $n_{in}$  and  $n_{out}$  as fitting parameters improves the Energy efficiency estimate for LLM inference w.r.t. considering only  $n_{out}$ . The two proposed analytical models (FLOPs-based and Memory-and-FLOPs-based) improves the MAPE over Baseline 4, reducing it to 2.27% ( $\pm 0.61$ ) and 1.79% ( $\pm 0.61$ ) respectively. This underlines that the proposed FLOPs based model derived from computational complexity estimates better captures the dependency of LLM inference Energy Efficiency w.r.t. SoA, and that this dependency is non linear with both quadratic and mixed terms dependencies. Furthermore, the proposed Memory-and-FLOPs-based consistently reduces the MAPE over the FLOPs-based one with an average reduction of the 18.6%, underlining that memory access operations are important as FLOPs and the fifth term in the analytical model is important. In particular, the quadratic term  $n_{in}^2$  can be interpreted as the initial cost incurred during the prefill phase. This cost dominates when the input sequence is relatively long, creating a high starting point in the per-token energy curve. As output tokens are generated, the cost reaches an optimal point where the amortization of input costs balances the linear per-token decoding costs. Beyond this optimum, the cost grows linearly with the number of output tokens, reflecting the sequential nature of decoding.

Finally, by examining the derivative of the per-token energy with respect to  $n_{out}$ , we can identify the points of maximal efficiency observed in the experiments. The derivative analysis confirms the presence of an optimal number of output tokens that minimizes the per-token energy, matching the peak efficiency points observed in the empirical data.

## 8 Current limitations and Future works

### 8.1 Experimental settings

The experimental evaluation presented in this work is subject to some limitations that should be acknowledged. First, our analysis focuses on relatively small-scale models, which may not fully capture the performance characteristics of larger LLMs with substantially

different parameter counts and memory footprints. Second, all experiments were conducted on a single hardware platform, limiting the generalizability of the results across heterogeneous systems with different compute, memory, and interconnect properties. Finally, we relied on a single serving framework, which constrains the scope of our conclusions, as alternative serving solutions may employ different optimization strategies and execution models that affect performance.

Future work will address these limitations by extending the experimental study to a broader range of model sizes, including large-scale and emerging LLM architectures, and by evaluating performance across multiple hardware platforms. In addition, incorporating multiple serving frameworks will allow a more systematic comparison of software-level optimizations and requests scheduling strategies. Developing a more generalized performance model that jointly accounts for compute- and memory-bound costs would provide a more comprehensive framework for predicting LLM serving efficiency and for guiding optimization strategies across a wider range of models and deployment scenarios.

### 8.2 Batch size characterization

The proposed analytical model does not explicitly account for the batch size, instead assuming a fixed maximum batch size by setting `max_batch_size` to 1024 for all evaluations.

As shown in Figure 1, the number of concurrent requests has a strong impact on Energy Efficiency, particularly at peak values, as the engine is able to process a larger number of requests simultaneously. To analyze the interaction between batch size and the number of requests, Figure 4 reports the Energy Efficiency of Llama 3.2 1B while varying the maximum batch size configuration (`max_batch_size`) across a range of values: 64, 128, 256, 512 and 1024. We tested these configurations for two different workloads, namely  $N_{req} = 128$  and  $N_{req} = 1000$ , with the input sequence length fixed to  $n_{in} = 64$ .

As shown in Figure 4a, setting a maximum batch size larger than the number of requests (128) does not provide any efficiency benefit. Conversely, smaller batch sizes, such as 64, lead to a significant reduction in efficiency, as they prevent the engine from forming larger batches, resulting in under utilization of computational resources.

When considering a higher number of requests ( $N_{req} = 1000$ ), as illustrated in Figure 4b, the maximum batch size has a strong effect on overall efficiency. In particular, the peak efficiency decreases from 120.71 with a batch size of 1024 to 48.90 when the batch size is reduced to 64. However, the impact of the batch size diminishes for longer output sequences. For instance, when  $n_{out} = 4096$ , the efficiency gap between batch sizes of 256 and 1024 narrows to 47.27 and 51.91, respectively. This reduced sensitivity to batch size is attributable to the decode phase becoming dominant in requests with short inputs and long outputs, causing the engine to be constrained primarily by memory bandwidth rather than by the batch dimension.

In future work, we plan to extend our analysis of the impact of maximum batch size on LLM Energy Efficiency and to explicitly incorporate this parameter into the proposed analytical model.

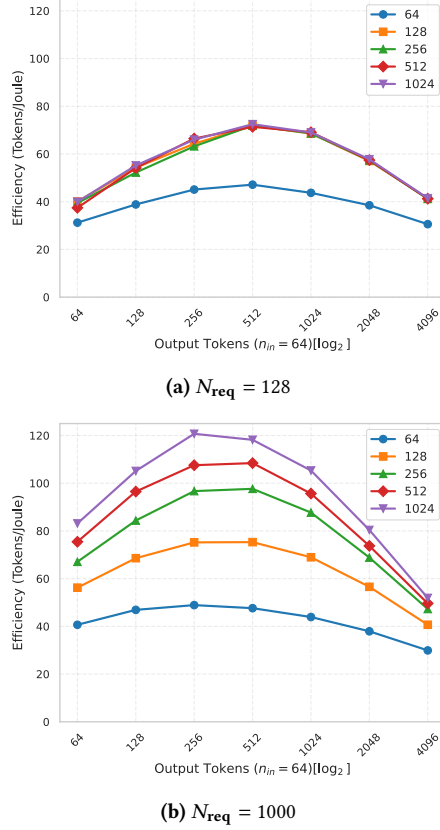


**Figure 4: Energy efficiency of Llama 3.2 1B varying maximum batch size considering different number of requests.**

## 9 Conclusions

This paper presented a comprehensive study of the Energy Efficiency of LLM inference evaluated on NVIDIA H100 GPUs with TensorRT-LLM. We showed that energy consumption during inference can be explained by decomposing FLOPs and Memory Access contributions into prefill and decode phases, and by normalizing them on a per-token basis. The resulting analytical model highlights the quadratic overhead of input processing, the amortization effect of output length, and the linear cost of sequential decoding. Our experiments confirm that this model aligns closely with real-world energy measurements. Specifically, we identified efficiency regimes where energy-per-token reaches a minimum, and demonstrated that these correspond to the balance point where input costs are sufficiently amortized without incurring excessive decoding overhead. This explains why efficiency peaks at short-to-moderate input lengths and medium outputs, while dropping significantly for long prompts or short generations.

Beyond theoretical insight, our findings have practical implications for LLM deployment. The analytical structure of inference costs allow to foresee efficiency Sweet Spots and to adapt prompt or generation length to reduce energy consumption. This perspective transforms Energy Efficiency from an empirical concept into a predictable design parameter. Building a generalized compute–memory

efficiency model will further broaden the applicability, supporting sustainable optimization across different architectures and deployment contexts. In summary, our study represents an intermediate step between empirical benchmarking and theoretical modeling of LLM inference costs, providing a model that not only explains current efficiency regimes but also guides more energy-aware deployment strategies for large-scale generative AI.

## References

Joshua Ainslie, James Lee-Thorp, Michiel de Jong, Yury Zemlyanskiy, Federico Lebrón, and Sumit Sanghi. 2023. GQA: Training Generalized Multi-Query Transformer Models from Multi-Head Checkpoints. *arXiv:2305.13245 [cs.CL]* <https://arxiv.org/abs/2305.13245>

Ebtiesam Almazrouei, Hamza Alobeidli, Abdulaziz Alshamsi, Alessandro Cappelli, Ruxandra Cojocaru, Mérourane Debbah, Étienne Goffinet, Daniel Hesslow, et al. 2023. The Falcon Series of Open Language Models. *arXiv:2311.16867 [cs.CL]* <https://arxiv.org/abs/2311.16867>

Reza Yazdani Aminabadi, Samyam Rajbhandari, Minjia Zhang, Ammar Ahmad Awan, Cheng Li, Du Li, Elton Zheng, Jeff Rasley, Shaden Smith, Olatunji Ruwase, and Yuxiong He. 2022. DeepSpeed Inference: Enabling Efficient Inference of Transformer Models at Unprecedented Scale. *arXiv:2207.00032 [cs.LG]* <https://arxiv.org/abs/2207.00032>

Andrea Bartolini, Francesco Beneventi, Andrea Borghesi, Daniele Cesarini, Antonio Libri, Luca Benini, and Carlo Cavazzoni. 2019. Paving the way toward energy-aware and automated datacentre. In *Workshop Proceedings of the 48th International Conference on Parallel Processing*, 1–8.

NVIDIA Corporation. 2025. Python Bindings for NVIDIA Management Library (pynvml). <https://pypi.org/project/nvidia-ml-py3/>. Accessed: 2025-09-12.

Tri Dao, Daniel Y. Fu, Stefano Ermon, Atri Rudra, and Christopher Ré. 2022. FlashAttention: Fast and Memory-Efficient Exact Attention with IO-Awareness. *arXiv:2205.14135 [cs.LG]* <https://arxiv.org/abs/2205.14135>

Jared Fernandez, Clara Na, Vashisth Tiwari, Yonatan Bisk, Sasha Luccioni, and Emma Strubell. 2025. Energy Considerations of Large Language Model Inference and Efficiency Optimizations. *arXiv:2504.17674 [cs.CL]* <https://arxiv.org/abs/2504.17674>

Aaron Grattafiori, Abhimanyu Dubey, Abhinav Jauhri, Abhinav Pandey, Abhishek Kadian, Ahmad Al-Dahle, Aiesha Letman, Akhil Mathur, et al. 2024. The Llama 3 Herd of Models. *arXiv:2407.21783 [cs.AI]* <https://arxiv.org/abs/2407.21783>

Nidhal Jegham, Marwan Abdelatti, Lassad Elmoubarki, and Abdeltawab Hendawi. 2025. How Hungry is AI? Benchmarking Energy, Water, and Carbon Footprint of LLM Inference. *arXiv:2505.09598 [cs.CY]* <https://arxiv.org/abs/2505.09598>

Wooseok Kwon, Zhuohan Li, Siyuan Zhuang, Ying Sheng, Liannmin Zheng, Cody Hao Yu, Joseph E. Gonzalez, Hao Zhang, and Ion Stoica. 2023. Efficient Memory Management for Large Language Model Serving with PagedAttention. *arXiv:2309.06180 [cs.LG]* <https://arxiv.org/abs/2309.06180>

Paul Joe Maliakel, Shashikant Ilager, and Ivona Brandic. 2025. Investigating Energy Efficiency and Performance Trade-offs in LLM Inference Across Tasks and DVFS Settings. *arXiv:2501.08219 [cs.LG]* <https://arxiv.org/abs/2501.08219>

Mayank Mishra, Matt Stallone, Gaoyuan Zhang, Yikang Shen, Aditya Prasad, Adriana Meza Soria, Michele Merler, Parameswaran Selvam, et al. 2024. Granite Code Models: A Family of Open Foundation Models for Code Intelligence. *arXiv:2405.04324 [cs.AI]* <https://arxiv.org/abs/2405.04324>

Chenxu Niu, Wei Zhang, Yongjian Zhao, and Yong Chen. 2025. Energy Efficient or Exhaustive? Benchmarking Power Consumption of LLM Inference Engines. *SIGENERGY Energy Inform. Rev.* 5, 2 (Aug. 2025), 56–62. doi:10.1145/3757892.3757900

NVIDIA. 2025. TensorRT-LLM. <https://github.com/NVIDIA/TensorRT-LLM>. Version 0.2.10, accessed September 15, 2025.

Samyam Rajbhandari, Jeff Rasley, Olatunji Ruwase, and Yuxiong He. 2020. ZeRO: Memory Optimizations Toward Training Trillion Parameter Models. *arXiv:1910.02054 [cs.LG]* <https://arxiv.org/abs/1910.02054>

Noam Shazeer. 2019. Fast Transformer Decoding: One Write-Head is All You Need. *CoRR abs/1911.02150* (2019), 0. arXiv:1911.02150 <http://arxiv.org/abs/1911.02150>

Jovan Stojkovic, Esha Choukse, Chaojie Zhang, Inigo Goiri, and Josep Torrellas. 2024. Towards Greener LLMs: Bringing Energy-Efficiency to the Forefront of LLM Inference. *arXiv:2403.20306 [cs.AI]* <https://arxiv.org/abs/2403.20306>

Gemma Team, Thomas Mesnard, Cassidy Hardin, Robert Dadashi, Surya Bhupatiraju, Shreya Pathak, Laurent Sifre, Morgane Rivière, et al. 2024. Gemma: Open Models Based on Gemini Research and Technology. *arXiv:2403.08295 [cs.CL]* <https://arxiv.org/abs/2403.08295>

Ashish Vaswani, Noam Shazeer, Niki Parmar, Jakob Uszkoreit, Llion Jones, Aidan N. Gomez, Łukasz Kaiser, and Illia Polosukhin. 2017. Attention is all you need. In *Proceedings of the 31st International Conference on Neural Information Processing Systems* (Long Beach, California, USA) (NIPS’17). Curran Associates Inc., Red Hook, NY, USA, 6000–6010.

Chen Wang, Jialin Qiao, Xiangdong Huang, Shaoxu Song, Haonan Hou, Tian Jiang, Lei Rui, Jianmin Wang, et al. 2025. Apache IoTDB: A Time Series Database for Large Scale IoT Applications. *ACM Trans. Database Syst.* 50, 2, Article 7 (May 2025), 45 pages. doi:10.1145/3726523

Patrick Wilhelm, Thorsten Wittkopp, and Odej Kao. 2025. Beyond Test-Time Compute Strategies: Advocating Energy-per-Token in LLM Inference. In *Proceedings of the 5th Workshop on Machine Learning and Systems* (World Trade Center, Rotterdam, Netherlands) (*EuroMLSys '25*). Association for Computing Machinery, New York, NY, USA, 208–215. doi:10.1145/3721146.3721953

Grant Wilkins, Srinivasan Keshav, and Richard Mortier. 2024. Offline Energy-Optimal LLM Serving: Workload-Based Energy Models for LLM Inference on Heterogeneous Systems. arXiv:2407.04014 [cs.DC] <https://arxiv.org/abs/2407.04014>

Thomas Wolf, Lysandre Debut, Victor Sanh, Julien Chaumond, Clement Delangue, Anthony Moi, Pierrick Cistac, Tim Rault, Rémi Louf, Morgan Funtowicz, Joe Davison, Sam Shleifer, Patrick von Platen, Clara Ma, Yacine Jernite, Julien Plu, Canwen Xu, Teven Le Scao, Sylvain Gugger, Mariama Drame, Quentin Lhoest, and Alexander M. Rush. 2020. Transformers: State-of-the-Art Natural Language Processing. In *Proceedings of the 2020 Conference on Empirical Methods in Natural Language Processing: System Demonstrations*. Association for Computational Linguistics, Online, 38–45. <https://www.aclweb.org/anthology/2020.emnlp-demos.6>

An Yang, Baosong Yang, Binyuan Hui, Bo Zheng, Bowen Yu, Chang Zhou, Chengpeng Li, Chengyuan Li, et al. 2024. Qwen2 Technical Report. arXiv:2407.10671 [cs.CL] <https://arxiv.org/abs/2407.10671>

Zhihang Yuan, Yuzhang Shang, Yang Zhou, Zhen Dong, Zhe Zhou, Chenhao Xue, Bingzhe Wu, Zhikai Li, Qingyi Gu, Yong Jae Lee, Yan Yan, Beidi Chen, Guangyu Sun, and Kurt Keutzer. 2024. LLM Inference Unveiled: Survey and Roofline Model Insights. arXiv:2402.16363 [cs.CL] <https://arxiv.org/abs/2402.16363>

Susan Zhang, Stephen Roller, Naman Goyal, Mikel Artetxe, Moya Chen, Shuohui Chen, Christopher Dewan, Mona Diab, et al. 2022. OPT: Open Pre-trained Transformer Language Models. arXiv:2205.01068 [cs.CL] <https://arxiv.org/abs/2205.01068>

## A Appendix

This appendix provides additional quantitative details supporting the modeling and statistical analysis presented in the main body of

the paper. In particular, it reports the full set of regression parameters significance statistics and values for the proposed *Memory and FLOPs based* analytical model across all evaluated LLMs.

### A.1 Parameters significance

Table 4 summarizes the aggregated statistical significance of each model parameter across all evaluated LLMs. By reporting the distribution of  $p$ -values for each parameter, this table highlights which components of the model consistently contribute to explaining performance variation and which parameters exhibit weaker or model-dependent influence. Together, these tables complement the main results by offering a detailed view of the model fitting behavior and its statistical robustness across different architectures and scales. In the table, the number asterisks quantify the significance of the parameter, with (\*\*\*) meaning high significance, (\*\*) moderate significance, (\*) weaker significance and n.s. not significant.

### A.2 Parameters value

Table 5 lists the fitted values of the model parameters  $\theta_0$ – $\theta_5$  for each LLM, grouped by scale. In addition, it reports both the empirically observed sweet spots and the corresponding values estimated by the proposed model, enabling a direct comparison between measured and predicted optimal configurations. These results provide transparency into the parameterization of the model and allow reproducibility of the sweet-spot estimation process.

**Table 4: Aggregated statistical significance across LLM datasets.**

Parameter	$p < 0.001$ (***)	$p < 0.01$ (**)	$p < 0.05$ (*)	$p \geq 0.05$ (n.s.)
$\theta_0$	13/13 (100%)	0/13 (0%)	0/13 (0%)	0/13 (0%)
$\theta_1$	13/13 (100%)	0/13 (0%)	0/13 (0%)	0/13 (0%)
$\theta_2$	13/13 (100%)	0/13 (0%)	0/13 (0%)	0/13 (0%)
$\theta_3$	13/13 (100%)	0/13 (0%)	0/13 (0%)	0/13 (0%)
$\theta_4$	13/13 (100%)	0/13 (0%)	0/13 (0%)	0/13 (0%)
$\theta_5$	8/13 (62%)	1/13 (8%)	3/13 (23%)	1/13 (8%)

**Table 5: Theta values and Sweet-Spots estimation for our Memory and FLOPs based model. (Percentages may not sum to 100% due to rounding)**

Model	$\theta_0$	$\theta_1$	$\theta_2$	$\theta_3$	$\theta_4$	$\theta_5$	Sweet Spot	Sweet Spot (Estimated)
<b>XS models</b>								
Llama 3.2 (1B)	5.005153e-03	1.079941e-07	6.825240e-06	2.611042e-03	3.852659e-06	5.406443e-01	64/256	64/429
OPT (1.3B)	5.969229e-03	1.666292e-07	4.388860e-05	2.915735e-03	2.342971e-05	3.187084e-01	64/64	64/147
Qwen 2 (1.5B)	6.528509e-03	9.147483e-08	6.199954e-06	3.700520e-03	3.288754e-06	3.805096e-01	64/512	64/433
<b>S models</b>								
Gemma 2 (2B)	9.468873e-03	1.223718e-07	2.486662e-05	5.371303e-03	1.372551e-05	5.856132e-01	64/256	64/260
OPT (2.7B)	6.541956e-03	2.855932e-07	9.197051e-05	5.909706e-03	5.038964e-05	8.566784e-01	64/128	64/157
Llama 3.2 (3B)	9.259155e-03	1.842970e-07	2.709305e-05	6.842019e-03	1.461407e-05	8.942031e-01	64/256	64/302
Granite (3B)	9.300161e-03	4.210179e-07	9.340093e-05	7.914036e-03	5.199433e-05	1.170166e+00	64/128	64/180
<b>M models</b>								
OPT (6.7B)	1.300082e-02	4.308046e-07	1.440099e-04	1.379572e-02	8.632801e-05	1.016691e+00	64/128	64/148
Qwen 2 (7B)	1.857219e-02	2.598309e-07	1.531846e-05	1.465957e-02	9.735924e-06	8.719728e-01	64/512	64/431
Falcon-RW (7.5B)	1.871769e-02	9.200243e-07	1.652377e-04	1.673305e-02	1.052294e-04	7.410144e-01	64/128	64/131
Granite (8B)	2.073270e-02	3.926489e-07	4.029094e-05	1.744363e-02	2.512785e-05	8.540071e-01	64/256	64/280
Llama 3.1 (8B)	1.970934e-02	3.329326e-07	3.583505e-05	1.551942e-02	2.249613e-05	8.939092e-01	64/256	64/290
Gemma 2 (9B)	1.749322e-02	5.981696e-07	1.110917e-04	1.901597e-02	7.408055e-05	2.558409e+00	64/64	64/226